



Supplement of

Earthquake ruptures and topography of the Chilean margin controlled by plate interface deformation

Nadaya Cubas et al.

Correspondence to: Nadaya Cubas (nadaya.cubas@sorbonne-universite.fr)

The copyright of individual parts of the supplement might differ from the article licence.

Inversion procedure:

Observed data:

Observed data are the topographic slopes (α^{obs}) and the slab dips (β^{obs}). We use ETOPO 1 (Amante and Eakins, 2009) to derive the bathymetric and topographic slopes, and slab 2.0 for the slab dips (Hayes et al., 2018). We build swath profiles perpendicular to the trench every 0.1 degree along a NS transect (Fig. **S1**), smoothed by a rectangular window of 25 km wide, following Cubas et al. (2013), to get averaged topographic slopes and slab dips with their standard deviations (Fig. **3** and **S2**) necessary to the inversion procedure.

Model space exploration:

The parameter space is composed of the effective basal friction (ϕ_b^{eff}), the wedge internal friction (ϕ_{int}) and the internal pore pressure ratio (λ). We assume a density of 2600kg/m³ and the three model parameters are explored from 10 to 45° every 0.25° for ϕ_{int} , from 1 to 44.9° every 0.1° for ϕ_b^{eff} , from 0.35 to 0.975 every 0.025 for λ .

Along each $\alpha - \beta$ profile, we select segments with slopes comprised in between the two extreme theoretical envelopes of the parameter space. For each segment, we explore the whole parametric space grid.

Direct problem:

Along a segment, for each point of the sampling (n), we calculate the predicted dip angle of the megathrust, β^{calc} for the observed topographic slope α_{obs} , based on the critical taper theory (Dahlen, 1984).

Comparison between observed and calculated data:

We evaluate the merit of each set of model parameters by comparing the predicted, β^{calc} , and observed, β^{obs} , values of the taper angle with a L2 norm (assuming a gaussian distribution of errors). The uncertainty on the taper angle is $\sigma = \sigma_{\beta_{obs}} + \sigma_{\alpha}$ including the contribution of the uncertainties on the topographic slope, $\sigma_{\alpha_{obs}}$ and dip angle $\sigma_{\beta_{obs}}$ on the predicted taper angle.

The misfit M function calculated for each point of the sampling (n) is then:

$$M_{\beta} = \frac{1}{n+1} \sum_{i=1}^n \frac{1}{2} \frac{(\beta^{obs}(i) - \beta^{calc}(i))^2}{(\sigma(i))^2}. \quad (1)$$

The probability density distribution of the model parameters is computed based on the misfit, following (Tarantola, 2005):

$$P(\phi_{int}, \phi_b^{eff}, \lambda) = \frac{1}{K} e^{-M(\phi_{int}, \phi_b^{eff}, \lambda)}, \quad (2)$$

with K the constant normalization factor of the probability over the model space:

$$K = \int_{\phi_{int}} \int_{\phi_b^{eff}} \int_{\lambda} e^{-M(\phi_{int}, \phi_b^{eff}, \lambda)} d\phi_{int} d\phi_b^{eff} d\lambda. \quad (3)$$

Since the probability density has three dimensions, to visualize the results, 1D marginal probabilities are calculated from integrations over two model space parameters (Fig. **S3**). These marginal probabilities provide the distributions of one parameter independently of others, also named 1D marginal probability density, for instance for ϕ_{int} :

$$P(\phi_{int}) = \int_{\phi_b^{eff}} \int_{\lambda} P(\phi_{int}, \phi_b^{eff}, \lambda) d\phi_b^{eff} d\lambda. \quad (4)$$

Figure **S4** shows the best misfits. We only kept segments with best misfits lower than 0.1, and with values consistent with standard frictions: from 25 to 43° for ϕ_{int} , consistent with lab experiment values (Byerlee, 1978), from 1 to 42.9° for ϕ_b^{eff} (same range as the internal friction but considering additional pore fluid pressure effect), and from 0.35 to 0.95 for λ . Results are compiled in the Table provided as a Suppl. Mat. ('Segment_results.dat').

Figure **1** is built from these results.

Best misfits of Figures **3** and **S2** are provided in Table **1**, and plotted on Figures **3** and **S2**.

Sensitivity tests were run by Cubas et al. (2013), showing that an error of $\pm 5^\circ$ on β implies a horizontal translation of the taper and a 3° variation for the effective basal friction, without affecting the critical state of the forearc. They also discuss the weak impact of the sliding window when lower than 40km wide (Fig. **S6**).

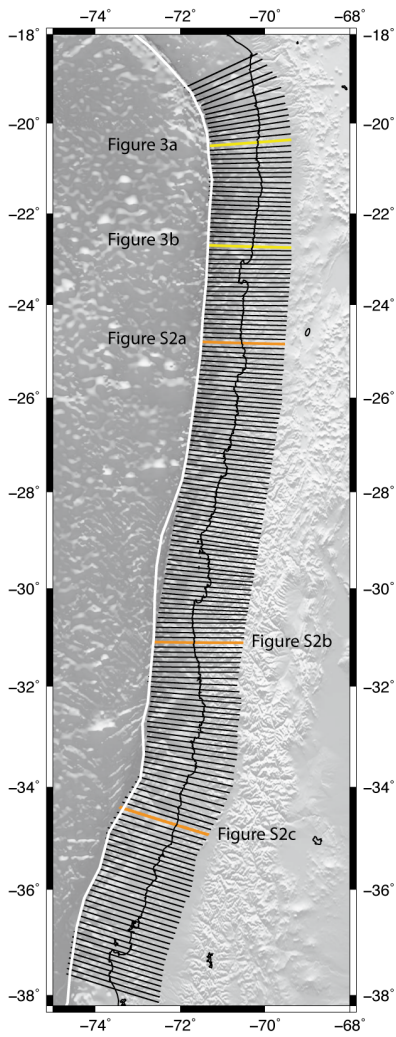


Figure 1: **S1** - Cross-sections used for inversion.

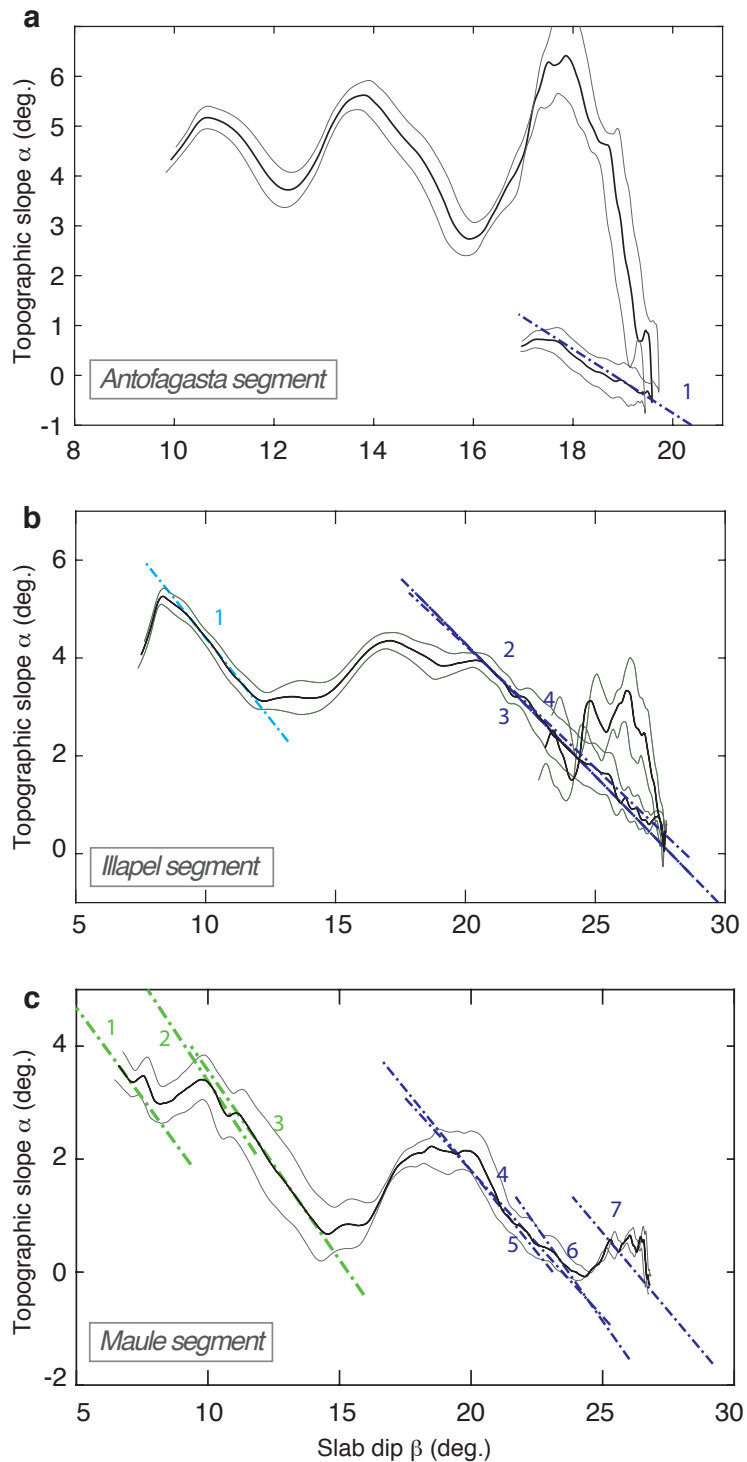


Figure 2: **S2** - Topographic slope (α) versus slab dip (β) for swath profiles along the a. Antofagasta, b. Illapel and c. Maule segments (locations on Figure **S1**). Segments at critical state, according to inversion, are shown in green: when accretion, in blue: light blue when probably erosive, dark blue for probable underplating. Grey: swath plus or minus standard deviation. Properties of each segment are provided in Table **T1**.

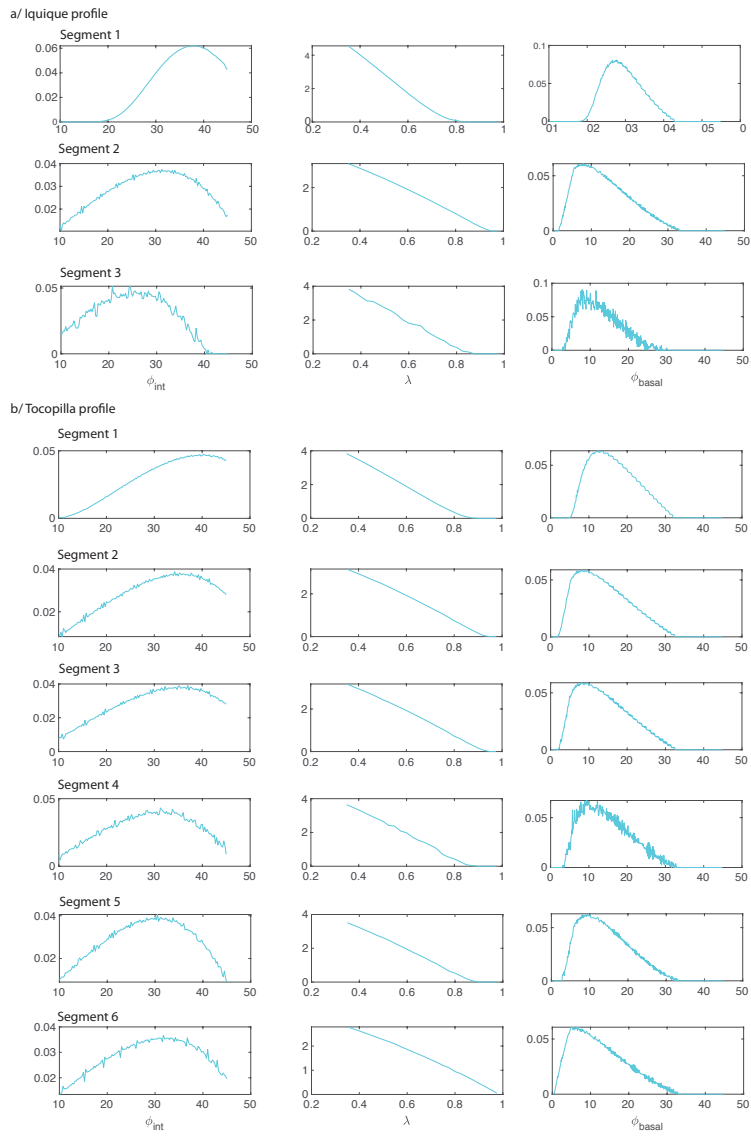


Figure 3: **S3** - Marginals 1D obtained for Figure **3a** and **3b** profiles.

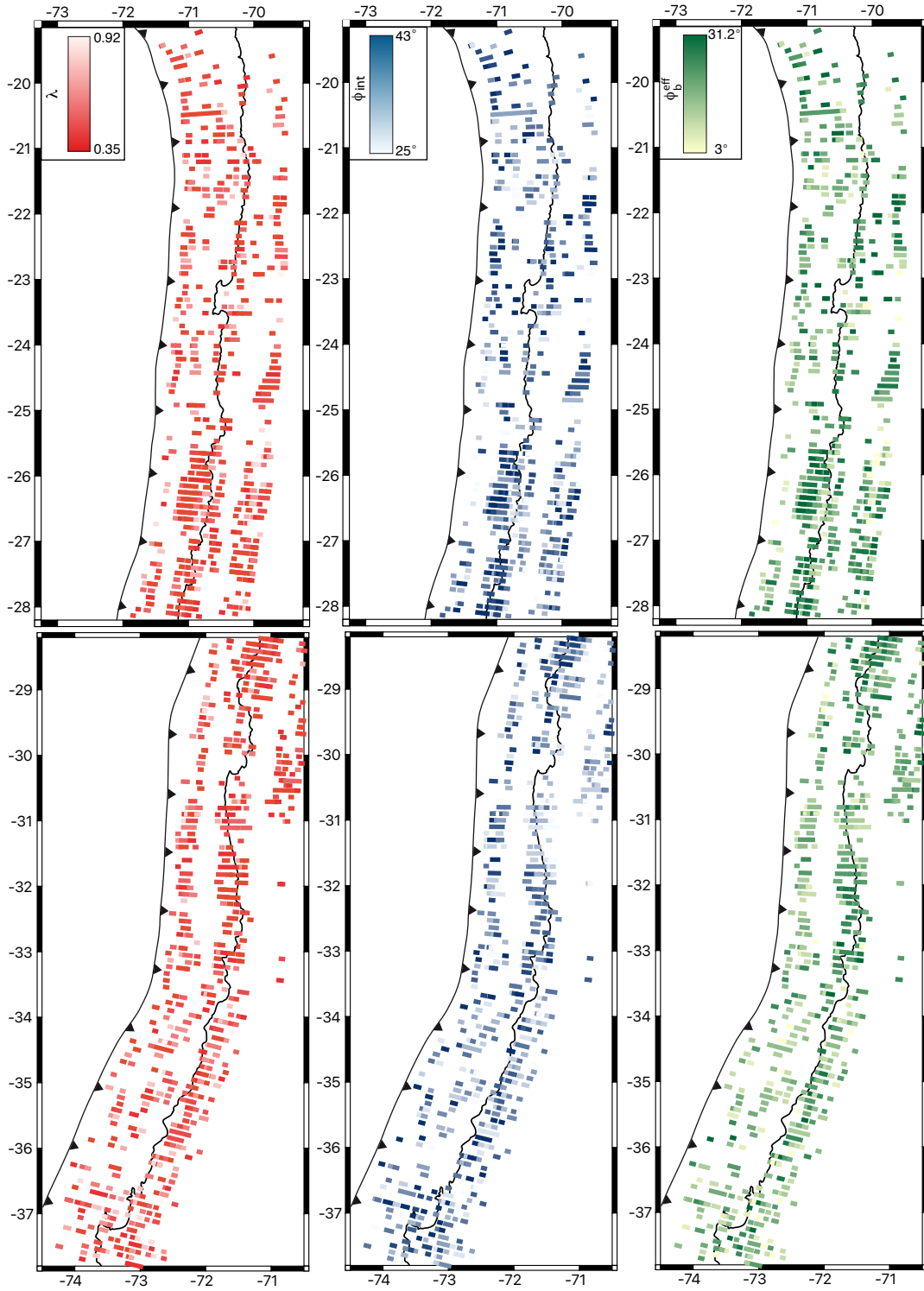


Figure 4: **S4** - Frictional properties of segments at critical state retrieved by inversion: Best misfits for internal pore pressure, internal friction angle and effective megathrust friction angle.

Table 1: **T1** - Best misfits of critical segments identified on figures **3** and **S2** (δ_b : angle between forward verging thrust and basal décollement).

| Cross-section | Internal pore pressure ratio λ | Internal friction angle ϕ_{int} ($^\circ$) | Effective basal friction angle ϕ_b^{eff} ($^\circ$) | Diff. of effective friction $\Delta\phi$ ($^\circ$) | Diff. of dip δ_b ($^\circ$) |
|--------------------|---|--|---|--|---|
| Iquique | | | | | |
| 1 | 0.35 | 33.75 | 22 | 1.47 | 8.1 |
| 2 | 0.775 | 35.5 | 8.8 | 0.3 | 5.8 |
| 3 | 0.35 | 27.25 | 17.0 | 0.15 | 9.8 |
| Tocopilla | | | | | |
| 1 | 0.7 | 42.25 | 14.7 | 0.54 | 5.3 |
| 2 | 0.85 | 41.5 | 7.4 | 0.16 | 4.1 |
| 3 | 0.5 | 32.5 | 16.0 | 1.67 | 9.7 |
| 4 | 0.35 | 40.5 | 28.7 | 0.33 | 3.4 |
| 5 | 0.625 | 31.75 | 12.6 | 0.46 | 6.2 |
| 6 | 0.775 | 38.75 | 9.8 | 0.43 | 6.1 |
| Antofagasta | | | | | |
| 1 | 0.475 | 30.75 | 15.4 | 1.94 | 10.8 |
| Illapel | | | | | |
| 1 | 0.625 | 38.75 | 15.1 | 1.65 | 9.0 |
| 2 | 0.575 | 27.75 | 12.5 | 0.1 | 3.2 |
| 3 | 0.575 | 25.25 | 11.2 | 0.13 | 6.4 |
| 4 | 0.575 | 25.25 | 11.2 | 0.13 | 6.4 |
| Maule | | | | | |
| 1 | 0.35 | 27.25 | 12 | 6. | 19 |
| 2 | 0.575 | 39.75 | 16.8 | 2.67 | 10.3 |
| 3 | 0.4 | 30.75 | 15.6 | 4.04 | 14.3 |
| 4 | 0.5 | 27.25 | 13.6 | 0.84 | 8.2 |
| 5 | 0.65 | 29.0 | 10.5 | 0.48 | 7.0 |
| 6 | 0.6 | 37.25 | 16.8 | 0.12 | 2.7 |
| 7 | 0.525 | 26.5 | 13 | 0.32 | 5.5 |

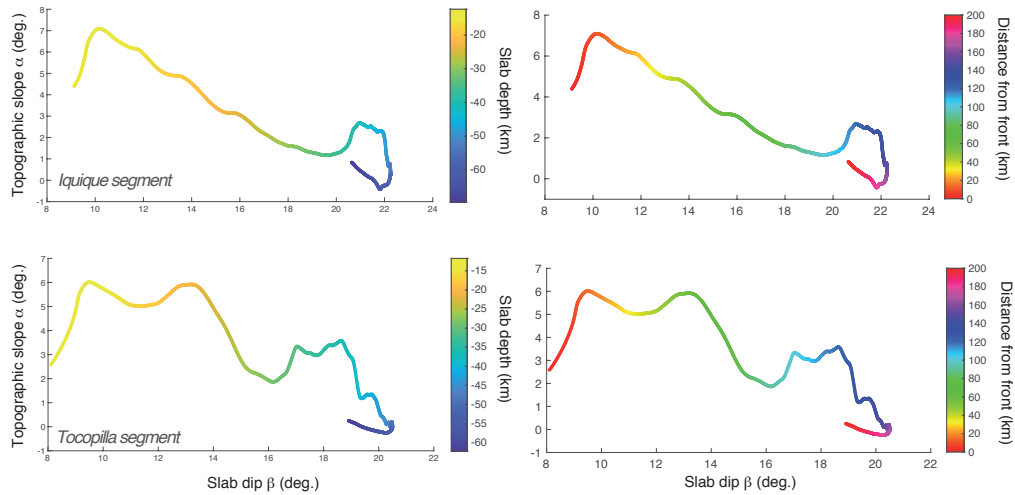


Figure 5: **S5** - Topographic slope (α) versus slab dip (β) of Figure **3a** and **3b** profiles with depth evolution and distance from the front shown as a gradient of color.

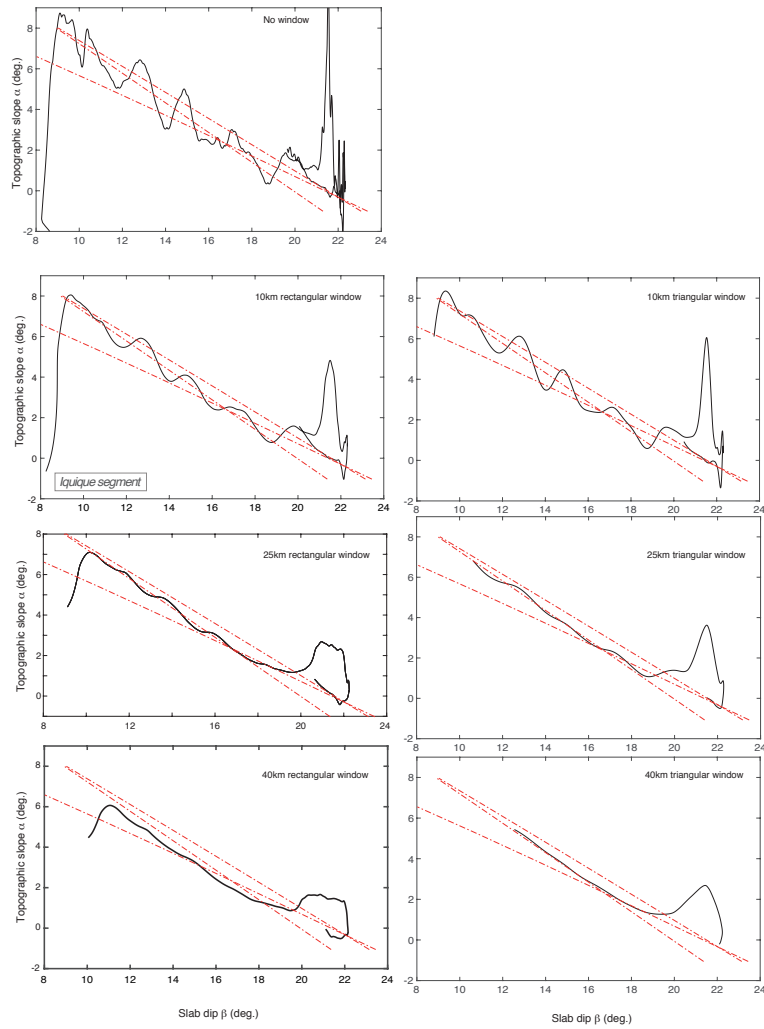


Figure 6: **S6** - Figure **3a** profile, original and smoothed topography by different window size (10, 25 and 40 km) and shape (rectangular, triangular). The critical areas are visible on original and smoothed data for both window shapes. The 25km large window allows keeping some topographic complexities and is smoothed enough to capture critical areas.

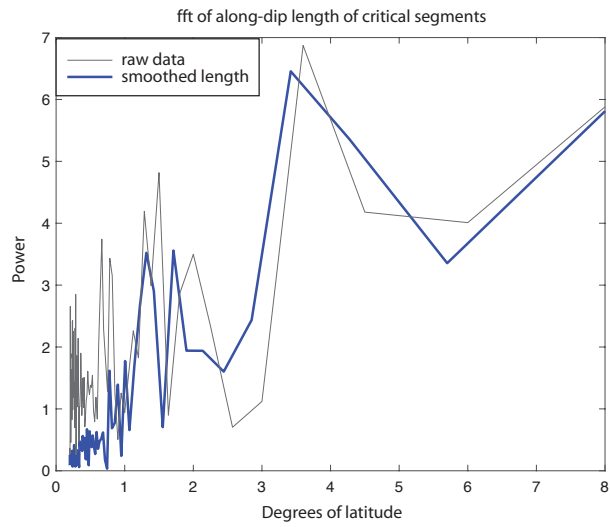


Figure 7: **S7** - FFT applied on raw and smoothed lengths of segments at critical state, as a function of latitude degrees. We can identify four major peaks: 8, 4, 2, 1.5°

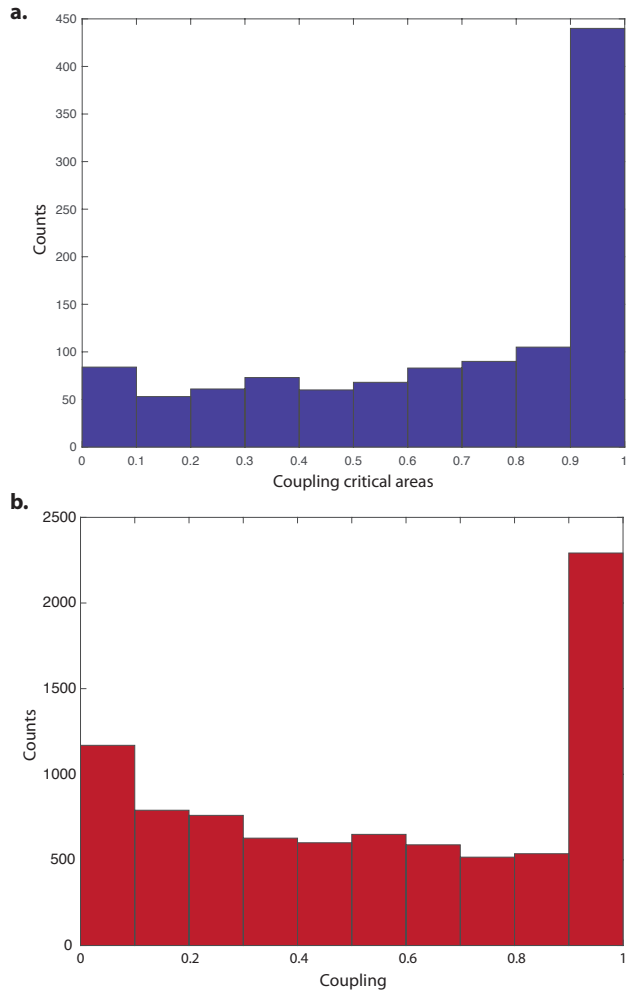


Figure 8: **S8** - Histograms of coupling values for a. critical segments and for b. Metois et al. (2016) model.

References

- Amante, C. and Eakins, B. W.: ETOPO1 arc-minute global relief model: procedures, data sources and analysis, 2009.
- Byerlee, J.: Friction of rocks, in: Rock friction and earthquake prediction, pp. 615–626, Springer, 1978.
- Cubas, N., Avouac, J.-P., Souloumiac, P., and Leroy, Y.: Megathrust friction determined from mechanical analysis of the forearc in the Maule earthquake area, *Earth and Planetary Science Letters*, 381, 92–103, 2013.
- Dahlen, F.: Noncohesive critical Coulomb wedges: An exact solution, *Journal of Geophysical Research: Solid Earth*, 89, 10 125–10 133, 1984.
- Hayes, G. P., Moore, G. L., Portner, D. E., Hearne, M., Flamme, H., Furtney, M., and Smoczyk, G. M.: Slab2, a comprehensive subduction zone geometry model, *Science*, 362, 58–61, 2018.
- Tarantola, A.: *Inverse problem theory and methods for model parameter estimation*, SIAM, 2005.